



# Tagged deep inelastic scattering measurement on deuterium with the LAD experiment

F. Hauenstein<sup>1,a</sup>, C. Ayerbe Gayoso<sup>2</sup>, S. Ratliff<sup>3</sup>, H. Szumila-Vance<sup>1</sup>, A. Schmidt<sup>3</sup>, L. Ehinger<sup>4</sup>, O. Hen<sup>4</sup>, D. Higinbotham<sup>1</sup>, I. Korover<sup>6</sup>, T. Kutz<sup>4</sup>, D. Nguyen<sup>5</sup>, E. Piasetzky<sup>6</sup>, L. B. Weinstein<sup>2</sup>

<sup>1</sup> Thomas Jefferson National Accelerator Facility, Newport News, VA 23606, USA

<sup>2</sup> Old Dominion University, Norfolk, VA 23529, USA

<sup>3</sup> George Washington University, Washington, DC 20052, USA

<sup>4</sup> Massachusetts Institute of Technology, Cambridge, MA 02139, USA

<sup>5</sup> University of Tennessee, Knoxville, TN 37996, USA

<sup>6</sup> Tel Aviv University, Tel Aviv 69978, Israel

Received: 14 February 2024 / Accepted: 29 May 2024

© Jefferson Science Associates, LLC and Carlos Ayerbe Gayoso, Sara Ratliff, Axel Schmidt, Lucas Ehinger, Or Hen, Igor Korover, Tyler Kutz, Dien Nguyen, Eliezer Piasetzky, Lawrence B Weinstein, under exclusive licence to Società Italiana di Fisica and Springer-Verlag GmbH Germany, part of Springer Nature 2024

Communicated by Patrizia Rossi

**Abstract** The origin of the modification of the quark structure of nucleons in the nuclear medium can be tested with tagged recoil nucleon measurements from deep inelastic scattering off electrons on deuterium. The LAD experiment at the Thomas Jefferson National Laboratory (JLab) will measure the modification of the neutron structure function for high-momentum, highly-virtual neutrons by measuring the spectator recoil protons in coincidence with the scattered electron. An update on the experimental setup and projected results is presented. The experiment will collect data in Fall 2024.

## 1 Introduction

One of the outstanding questions in nuclear physics is how the quark structure of nucleons is modified in the nuclear medium. Evidence for nucleon modification comes from deep inelastic scattering (DIS) measurements of the ratio of per-nucleon cross sections of nucleus  $A$  to deuterium. These experiments typically measure a ratio of about 1 at Bjorken- $x = 0.3$ , decreasing linearly to a minimum at around  $x = 0.7$  [1, 2]. This minimum depends on  $A$  and varies from about 0.94 for He-4 to about 0.83 for gold. This observation is known as the EMC effect [3].

While the EMC effect has been studied in detail by various experiments [2–5], there is no generally accepted explanation of its origin. In recent years experimental results have strengthened the correlation of the size of the EMC effect in a given nucleus to the probability for a nucleon in that nucleus to belong to a short-range correlated pair (SRC) of nucleons [6, 7]. This strongly suggests that the EMC effect is due to high-momentum highly-virtual nucleons in nuclei. Since almost all high-momenta nucleons in nuclei belong to SRC nucleon pairs, we can select the nucleons on which we observe the EMC effect by detecting their SRC partners (tag) that recoil backwards in a deep inelastic scattering experiment with electrons.

Deuterium is the optimal system in which to study the dependence of the nucleon structure on the nucleon virtuality. The probability for a high momentum configuration in the deuterium is rather small relative to heavier nuclei but this configuration can be ‘tagged’ cleanly by the emission of a fast nucleon to the backward hemisphere. In a simple spectator picture with no final state interaction (FSI), the backward moving nucleon is a spectator, does not participate in the DIS process, and allows us to determine the virtuality of the nucleon from which the electron scattered. Two tagged experiments on deuterium are conducted at the Thomas Jefferson National Laboratory (JLab) utilizing the electron beam from the CEBAF accelerator [8] with energies up to 11 GeV. One of these experiments is measuring the modification of protons by tagging recoil neutrons and the other one is measuring the modification of neutrons by tagging recoil protons. The first one took data with the CLAS12 detector [9] at JLab exper-

The U.S. Government retains a non-exclusive, paid-up, irrevocable, world-wide license to publish or reproduce this manuscript for U.S. Government purposes.

<sup>a</sup> e-mail: [hauenst@jlab.org](mailto:hauenst@jlab.org) (corresponding author)

imental Hall B and a backward angle neutron detector [10], and initial results are under collaboration review. The later experiment is the focus of this article. It will be conducted in Fall of 2024 in JLab's experimental Hall C.

The main part of the experiment is a 1.5-sr Large Acceptance Detector (LAD) based on scintillator bars to detect the recoil protons. This detector gives the experiment its name - The LAD experiment. The electrons from the deep inelastic scattering are detected in the two magnetic spectrometer in Hall C. These are the legacy High Momentum Spectrometer (HMS, momentum acceptance  $\Delta p/p \pm 10\%$ , solid angle  $\Omega = 7$  msr) [11, 12] and the new Super High Momentum Spectrometer (SHMS, momentum acceptance  $\Delta p/p$  from  $-10$  to  $+12\%$ , solid angle  $\Omega = 4$  msr) [13].

In the original experiment proposal [14], the settings for the spectrometers and LAD were chosen based on a simulation that considered conditions expected in 2011 at the time of the proposal. Between then and now, a number of specific details about the LAD experiment have changed: A pair of GEM detectors from the first PRad experiment at JLab [15] is used for vertexing, the luminosity will be larger, and the placement of the LAD panels has been adjusted around space constraints in the experimental hall. In this article, we review the changes and give updated predictions for the results based on new simulations. The article is organized as follows: In Sect. 2, we give some background on the main observable measured in the experiment and we comment on the suppression of final state interactions with the planned experimental setup. The details of the setup are presented in Sect. 3. The updated projected results and theoretical predictions for the main observable are presented in Sect. 4.

## 2 Theoretical background

### 2.1 Double-ratio observable

The goal of the LAD experiment is to extract an observable that is sensitive to the structure of high-momentum neutrons within deuterium, and robust against systematic experimental effects. The observable of interest is a double-ratio of experimental to theoretical normalized yields for tagged DIS events. Theoretical yields are obtained from events generated with a theory cross section model and propagated through full GEANT simulations of the experiment.

For the reaction of interest, the yields are a function of four variables  $Y(Q^2, p_T, \alpha_S, x')$  (for a definition of variables see Appendix A), excluding the azimuthal angles of the electron and spectator proton, about which the cross section is symmetric. We integrate over the experimental acceptance in  $Q^2$  and transverse momentum  $p_T$ , reducing the yield to a function of two variables,  $Y(\alpha_S, x')$ .

In order to study the modification of bound neutron structure (dependent on  $x'$ ) as a function of neutron momentum

(dependent on  $\alpha_S$ ), we will bin the data in  $x'$  and examine the  $\alpha_S$  dependence in each bin. For a given bin  $\alpha_{S,i}$ , we normalize the yield to a fixed kinematic point  $x'_0$ . Therefore, we obtain the following double-ratio:

$$\mathcal{R}(\alpha_{S,i}, x') = \frac{Y_{exp}(\alpha_{S,i}, x')/Y_{exp}(\alpha_{S,i}, x'_0)}{Y_{sim}(\alpha_{S,i}, x')/Y_{sim}(\alpha_{S,i}, x'_0)} \quad (1)$$

$$= \frac{\sigma_{exp}(\alpha_{S,i}, x')/\sigma_{exp}(\alpha_{S,i}, x'_0)}{\sigma_{theory}(\alpha_{S,i}, x')/\sigma_{theory}(\alpha_{S,i}, x'_0)} \quad (2)$$

In the data analysis, we will choose the fixed kinematic point for normalization to be  $x'_0 \approx 0.3$ . While to some extent this is an arbitrary choice, inclusive measurements of the EMC effect in nuclei tend to be close to unity in the vicinity of  $x_B \approx 0.3$ , indicating the minimization (or at least large cancellation) of nuclear effects. Thus, we normalize to a point where one expects the EMC effect to be smallest.

The equality of Eqs. (1) and (2) is limited by how accurately the simulation models the experimental apparatus, physics effects (such as radiative corrections, detector resolution and bin migration, detector efficiencies, etc.) and how similar the theoretical cross section is to the experimental cross section. Previous experiments with the SHMS and HMS in Hall C have typically achieved systematic uncertainties of 4% or better in cross section measurements with the spectrometers [2, 16]. These uncertainties include the modeling of the spectrometer and the physics effects. In our experiment we will have additional systematic uncertainty from the modeling of the new detectors, LAD and the GEMs. We estimate this uncertainty to be 3% [14] giving a combined systematic uncertainty of 5% in our double-ratio in Eq. (2).

The double-ratio is proportional to the ratio of the bound-to-free-neutron structure functions under the assumptions of no rescattering of the recoil proton (i.e., PWIA) and the use of the free neutron structure function  $F_2^n$  in simulation models. This gives:

$$\mathcal{R}(\alpha_{S,i}, x') \propto \frac{F_2^{n*}(\alpha_{S,i}, x')/F_2^{n*}(\alpha_{S,i}, x'_0)}{F_2^n(\alpha_{S,i}, x')/F_2^n(\alpha_{S,i}, x'_0)} \quad (3)$$

The extraction of the structure function ratio in Eq. (3) has theoretical uncertainties from the knowledge of the free neutron structure function as well as the suppression of rescattering from final-State Interactions (FSI). We assume that the FSI uncertainty dominates, since we have good knowledge about the free neutron structure function from measurements by the BoNuS experiment at JLab [17], which will be improved further by upcoming results from the BoNuS12 experiment [18]. Details about FSI suppression and assigned uncertainty are discussed in the next section.

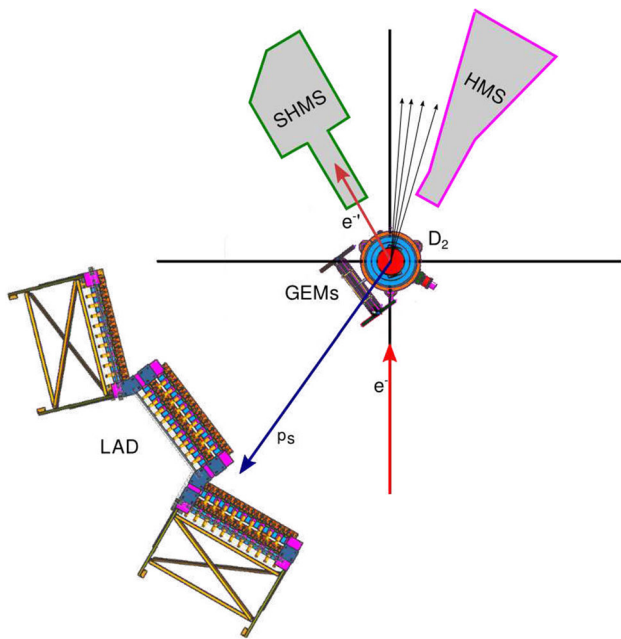


**Fig. 1** Sketch of experimental setup utilizing the CAD models of the LAD scintillator wall, GEMs and scattering chamber. The HMS and SHMS are shown for reference not at scale. A possible event is shown with a recoil proton to LAD and the scattered electron detected by the SHMS

## 2.2 Suppression of FSI

Final-state interactions are due to the interactions of the recoiling nucleon with the debris of the struck nucleon formed after the virtual photon absorption by a quark. Note that this is complicated by propagation and hadronization of the struck quark and of the residual system. While there is no complete theory of FSI in DIS, there are a number of phenomenological models for the deuteron. The magnitude of the FSI in the reaction  $d(e, e' p_s)$  has been calculated in several models using plane-wave impulse approximation [19], general eikonal approximation as fit to data [20], and with models for the debris-nucleon interaction cross sections [21]. The different model calculations agree that FSI increase with  $W'$  and decrease with momentum transfer  $Q^2$ . The FSI do not depend strongly on  $x'$ , thus the ratio of cross sections for two different value of  $x'$  is much less sensitive to FSI. Furthermore, all models show that FSI should be suppressed at backward spectator angles. This agreement is also supported by  $d(e, e' p_s)X$  data from CLAS [22]. Therefore, the detectors which measure the recoiling nucleons should be positioned at large scattering angles with respect to the incoming beam on the target.

We also estimated the remaining systematic uncertainty from FSI effects, after suppression, on the extraction of the structure function ratio in Eq. (3). Using the calculation that predicts the largest FSI contributions at the backward angles

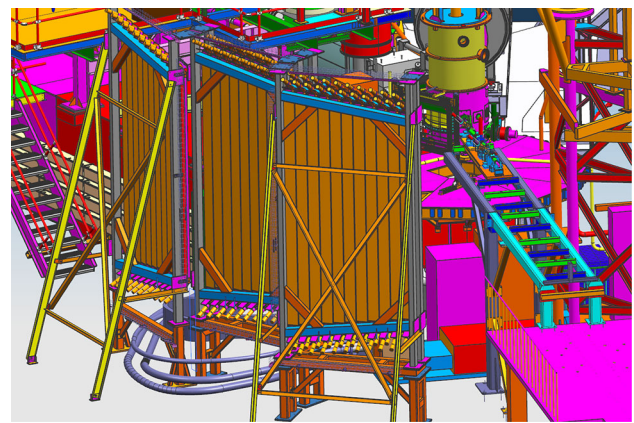


**Fig. 2** 3D model of the experimental setup in Hall C. The view is from behind the LAD detector in the direction of the target. The cyan and blue ladder structure on the right side indicates where the beam comes in

[21], we compare the ratio of cross section calculated with PWIA to the same ratio calculated with FSI. The difference between the ratio of PWIA+FSI cross sections and the ratio of PWIA cross sections at the proposed kinematics is about 4%, the entirety of which we take as a conservative estimate of the systematic uncertainty due to FSI effects.

## 3 Experimental setup

As mentioned, the general experimental setup has been updated from the initial proposal. A sketch of the new setup is shown in Fig. 1. In general, the experiment will measure simultaneously coincidence events of electrons detected in either the HMS or SHMS and recoil protons with momenta of 300–600 MeV/c detected in the GEMs and LAD. Due to space limitations in the experimental hall, the recoil detectors can only be placed on one side of the beam and the acceptance is limited to backward angles up to  $157^\circ$  by the exit window of the scattering chamber around the target. A 3D model of the hall and the detectors is shown in Fig. 2.

The incoming 11-GeV beam scatters off a 20-cm long, 2-cm wide and 2-cm high liquid deuterium target. The target is designed to not limit the acceptance of the outgoing particles. The scattering chamber around the target has two large exit windows which do not limit the in-plane angular acceptance of the electrons and recoil protons. However, the window for the protons limits the out-of-plane acceptance to  $\approx \pm 17^\circ$  which matches roughly the acceptance of LAD.

The HMS and SHMS momentum and central angle are changed throughout the experiment so that DIS electrons in different kinematics can be measured at the same time. Combined with the proton, these kinematics define low and high- $x'$  events. An overview of the different settings and associated beam time is given in Table 1. We will invert the settings on

**Table 1** Run plan and set-up configuration for the LAD experiment. Spectrometer angles indicating (L) or (H), for different production settings, correspond to kinematics at low- $x'$  ( $0.25 < x' < 0.35$ ) and

high- $x'$  ( $x' > 0.45$ ), respectively. The central values of  $Q^2$  for the L and H settings are 2.65 GeV<sup>2</sup> and 4.19 GeV<sup>2</sup>

		Target	HMS		SHMS		Current [ $\mu$ A]	Time
			$\theta$ [deg]	p[GeV/c]	$\theta$ [deg]	p[GeV/c]		
6.6 GeV	Commissioning and calibration	Empty	21.73	4.4	17	5.048	1	8 h
		LH2					10	24 h
10.9 GeV	Calibration	C foils	13.5	4.4	17	4.4	1	24 h
		C hole	13.5	4.4	17	4.4	10	24 h
		LD2	13.5	4.4	17	4.4	0.5–1.5	8 h
		Settings 1	LD2	13.5 (L)	4.4	17 (H)	4.4	1
	Settings 2	LD2	17 (H)	4.4	17 (H)	4.4	1	8 days
	Settings 3	LD2	17 (H)	4.4	13.5 (L)	4.4	1	8 days

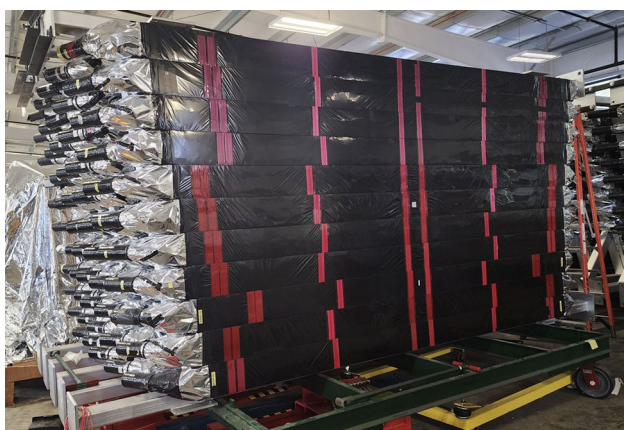


**Fig. 3** Picture of the LAD panels each consisting of eleven, 20-cm wide scintillator bars wrapped in black light-tight foil

the spectrometers to reduce systematic uncertainties in the measurement from the different spectrometer acceptances.

The LAD detector is assembled from approximately 4-m long scintillator counters of the former CLAS detector at Jefferson Lab [23, 24] after some refurbishing. Overall the detector consists of 55 scintillator bars which are readout on both sides with photo-multiplier tubes. The bars are arranged in 5 planes each with 11, 20-cm wide bars. The planes are organized in three stacks covering different scattering angles. The two stacks at larger angles consist each of two planes back-to-back to improve particle identification and background reduction in this angular range.

The bars will cover scattering angles from 90 to 157° at a distance of about 5–6 m from the target. Each bar is connected via fibers to a new laser calibration system similar to a system which was used in the BAND detector at Jefferson Lab [25]. The previously installed fibers on each bar had to be replaced due to damage over time. A significant amount of fibers were broken or scratched on one end. Further refurbishing has been carried out with the replacement

of PMTs or dividers on the bars since they reach the end of their lifetime after the old CLAS detector. In the experiment, the timing and value of deposit energy in the bars is used to perform particle identification, momentum determination and background reduction from pions.

To further reduce background, we will also track the charged particle trajectory with the GEM detectors which are positioned very close to the target chamber at distances of about 70–90 cm. The trajectory can be matched with bars which see a signal.

GEM detectors are designed to survive in high rate environments (few MHz/cm<sup>2</sup>) and yield typical tracking resolutions around 50 to 100  $\mu$ m. The two GEM layers in this experiment are repurposed from the PRad experiment [15] which were the largest GEM detectors at the time of their construction and assembly in 2015 at the University of Virginia [26]. Each GEM layer measures 120 by 55 cm<sup>2</sup> and is composed of a triple GEM foil assembly with 2 mm spacing between the foils, a drift cathode 3 mm above the first GEM amplification layer, and a readout board 2 mm below the last layer close to the readout. These GEMs demonstrated a tracking resolution  $\approx 70 \mu$ m in the PRad experiment and tracking efficiencies exceeding 95%. These GEM layers have an XY readout pattern with the readout strips connected to APV25 electronics front-end boards [27]. The APV chip samples six time samples at 40 MHz. The data is then readout through a Multi Purpose Digitizer (MPD) board. In anticipation of the high rate environments of this experiment, these GEMs have been configured with an individual channel power supply to supply voltage across the GEM foils. Also, an additional foil has been added externally to the GEM layers and in series with the cathode in order to prevent a gas window collapse due to high rate charge buildup.

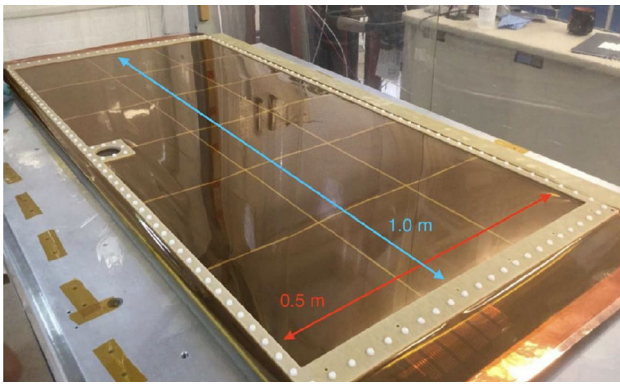


**Fig. 4** Picture of one layer of the GEM detectors used in the first PRAD experiment. They are about 1 m long and 0.5 m wide

### 4 Predictions

In 2020, as part of an experiment readiness review process, updated simulations were conducted that took into account the significant changes to the experiment since the writing of the original proposal (see Sect. 3). A Monte Carlo event generator was constructed using the plane-wave  $d(e, e' p_s)$  cross section calculation described in Ref. [20]. Particles in each event were propagated through a simplified model of the experiment geometry accounting for multiple scattering and the detector acceptance, and kinematic variables were smeared according to anticipated detector resolutions. Random coincidence background was also simulated, using the inclusive electron cross section model in Ref. [20], combined with an assumed inclusive proton cross section of  $1.43 \mu\text{b/sr}$ , a conservative estimate based on previous JLab data as well as Geant4-based radiation studies. The anticipated statistical and systematic uncertainty of the LAD experiment, including that due to random coincidence background subtraction, estimated from this simulation is shown in Fig. 5. The estimated systematic uncertainty is a combination of 5% on the individual yields, primarily stemming from detector acceptance, and an uncertainty of 4% coming from the theoretical uncertainty on FSI effects (see Sect. 2).

Figure 5 also shows a range of predictions for the LAD experiment observable (Eqs. (2) and (3)) at  $x' = 0.6$  relative to a reference value of  $x' = 0.3$ . The curves labeled “Binding,” “Rescaling” and “PLC Suppression” (for point-like configuration suppression) are calculated from models described in Ref. [19], and were included in the original LAD proposal. The shaded bands are predictions based on a more recent convolution model with virtuality-dependent nucleon modification, taken from Ref. [28] (specifically the structure function, linear-in- $x$  modification approach). The size of the bands shows the  $1\sigma$  uncertainty. The two bands differ in their assumption for the free neutron structure function  $F_2^n$ , which is supplied as external input to the model. Model 1 assumes

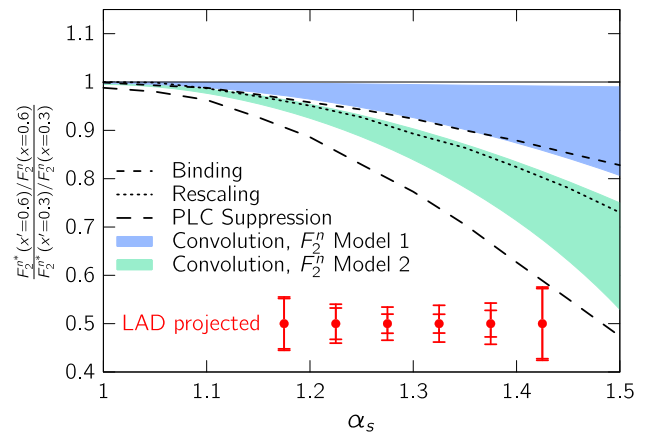


**Fig. 5** Theoretical predictions for the double ratio observable for LAD with inner error bars showing projected statistical uncertainty and outer error bars showing projected statistical and systematic uncertainty added in quadrature. The Binding, Rescaling, and PLC Suppression calculations are taken from Ref. [19]. The convolution calculations are taken from Ref. [28] under two different assumptions for the free neutron structure function  $F_2^n$ . Model 1 assumes an  $F_2^n/F_2^p$  ratio that behaves according to the results found in Ref. [29], while Model 2’s  $F_2^n/F_2^p$  behaves according to the results from Ref. [30]

a ratio  $F_2^n/F_2^p$  that behaves according to the results of Ref. [29]. Model 2 assumes that  $F_2^n/F_2^p$  behaves according to the results of Ref. [30]. Most analyses of  $F_2^n/F_2^p$  fall between these two results. As can be seen from the figure, LAD has the potential to refute some of the models about nucleon modification, and, possibly add an indirect constraint on the free neutron structure function.

### 5 Summary

Tagged deep inelastic scattering measurements on deuterium are a great tool to study the modification of quarks in nucleons. The upcoming LAD experiment will determine the structure function modification of high-momentum, highly-virtual neutrons in terms of a double-ratio observable which reduces systematic uncertainties. Over the last years, the experimental setup has been optimized compared to the initial proposal. The updated projection of the anticipated statistical and systematic uncertainties shows that the experiment has the potential to refute some of the models about the underlying mechanism of quark modification in nuclei and thus the origin of the EMC effect.

**Acknowledgements** This research was funded in part by Department of Energy (DOE) grant number DE-AC05-06OR23177 under which the Jefferson Science Associates operates the Thomas Jefferson National Accelerator Facility. Furthermore, the work was supported by the US Department of Energy Office of Science, Office of Nuclear Physics, under Award Numbers no. DE-FG02-96ER40960 and DE-SC0016583 and the OPRA, Pazy foundation, and the Israeli Science Foundation (917/20). The authors would like to thank the Jefferson Lab designers

and engineers Dean Spiers, Dan Young and Bert Metzger for their support in the update of the experimental setup and the design of required mechanical equipment for the installation of the detectors.

**Data Availability Statement** Data will be made available on reasonable request. [Author’s comment: Datasets are not yet available but will be available upon request.]

**Code Availability Statement** Code/software will be made available on reasonable request. [Author’s comment: Code to generate plots is available upon request.]

## Appendix A Definition of kinematic variables

From the scattered electron detected in SHMS or HMS, the standard inclusive kinematic variables can be reconstructed in terms of the four momentum of the initial electron  $k = (\vec{k}, E)$ , fixed target  $P = (0, M)$ , and scattered electron  $k' = (\vec{k}', E')$

$$\begin{aligned} \nu &= E - E' \\ Q^2 &= -q^2 = -(k - k')^2 \\ x_B &= \frac{Q^2}{2M\nu} \\ W^2 &= (P + q)^2 \end{aligned}$$

If a deep inelastic scattering event is tagged with a recoiling high-momentum proton with  $p_p = (\vec{p}_p, E_p)$ , one can construct variables sensitive to the neutron’s initial momentum within the nucleus. In the plane-wave impulse approximation (PWIA) the initial three-momentum of the bound neutron will be equal and opposite to the three-momentum of the recoiling spectator proton,  $\vec{p}_i = -\vec{p}_p$ . Fully defining the four-momentum is model-dependent, requiring some assumption on the off-shellness of the bound neutron. It is typical to define the bound neutron’s four-momentum as  $p_i = (-\vec{p}_p, m_D - E_p)$ . Tagged kinematic variables can then be reconstructed accounting for this Fermi motion:

$$\begin{aligned} (W')^2 &= (p_i + q)^2 \\ \alpha_S &= \frac{E_p - |\vec{p}_p| \cos \theta_{pq}}{M_p} \end{aligned}$$

The “primed” tagged variable  $W'$  is analogous to the inclusive  $W$ , but no longer assumes scattering from an at-rest nucleon. The variable  $\alpha_S$  is the lightcone momentum fraction of the spectator proton, and depends on  $\theta_{pq}$ , the angle between the recoiling proton and the virtual photon.  $p_T$  is the transverse momentum of the spectator proton with respect to the virtual photon direction.

Here we define the tagged scaling variable,  $x'$  (analog of  $x_B$ ) in terms of the invariant mass of the hadronic final state

recoiling against  $q$ :

$$x' = \frac{Q^2}{(W')^2 - M_p^2 + Q^2} \quad (\text{A1})$$

We note that there are other definitions of  $x'$  based on some assumption on the initial momentum of the bound nucleon.

## References

1. B. Schmookler et al., Modified structure of protons and neutrons in correlated pairs. *Nature* **566**(7744), 354–358 (2019). <https://doi.org/10.1038/s41586-019-0925-9>. arXiv:2004.12065 [nucl-ex]
2. A. Karki, D. Biswas, F.A. Gonzalez, W. Henry, C. Morean, A. Nadeeshani, A. Sun et al., First measurement of the emc effect in  $^{10}\text{B}$  and  $^{11}\text{B}$ . *Phys. Rev. C* **108**, 035201 (2023). <https://doi.org/10.1103/PhysRevC.108.035201>
3. J. Aubert et al., The ratio of the nucleon structure functions  $F_2^N$  for iron and deuterium. *Phys. Lett. B* **123**(3), 275–278 (1983). [https://doi.org/10.1016/0370-2693\(83\)90437-9](https://doi.org/10.1016/0370-2693(83)90437-9)
4. J. Gomez et al., Measurement of the A-dependence of deep inelastic electron scattering. *Phys. Rev. D* **49**, 4348–4372 (1994). <https://doi.org/10.1103/PhysRevD.49.4348>
5. J. Seely et al., New measurements of the EMC effect in very light nuclei. *Phys. Rev. Lett.* **103**, 202301 (2009). <https://doi.org/10.1103/PhysRevLett.103.202301>. arXiv:0904.4448 [nucl-ex]
6. L.B. Weinstein, E. Piassetzky, D.W. Higinbotham, J. Gomez, O. Hen, R. Shneor, Short range correlations and the EMC effect. *Phys. Rev. Lett.* **106**, 052301 (2011). <https://doi.org/10.1103/PhysRevLett.106.052301>. arXiv:1009.5666 [hep-ph]
7. O. Hen, E. Piassetzky, L.B. Weinstein, New data strengthen the connection between short range correlations and the EMC effect. *Phys. Rev. C* **85**, 047301 (2012). <https://doi.org/10.1103/PhysRevC.85.047301>. arXiv:1202.3452 [nucl-ex]
8. NP Continuous Electron Beam Accel... | U.S. DOE Office of Science (SC) <https://science.osti.gov/np/Facilities/User-Facilities/CEBAF> Electronically published 4 October 2023. Accessed 20 June 2024
9. V.D. Burkert et al., The CLAS12 spectrometer at Jefferson Laboratory. *Nucl. Instrum. Methods A* **959**, 163419 (2020). <https://doi.org/10.1016/j.nima.2020.163419>
10. E.P. Segarra et al., The CLAS12 backward angle neutron detector (BAND). *Nucl. Instrum. Methods A* **978**, 164356 (2020). <https://doi.org/10.1016/j.nima.2020.164356>. arXiv:2004.10339 [physics.ins-det]
11. *The HMS Spectrometer in Hall-C*. <https://www.jlab.org/physics/hall-c/hms>. Accessed 01 June 2024
12. C. Yero, PhD Thesis. <https://www.osti.gov/biblio/1644044>. Accessed 01 June 2024
13. D. Bhetuwal, J. Matter, H. Szumila-Vance, M.L. Kabir, D. Dutta, R. Ent, et al. Ruling out color transparency in quasielastic  $^{12}\text{C}(e, e'p)$  up to  $Q^2$  of 14.2 (GeV/c) $^2$ . *Phys. Rev. Lett.* **126**(8), 082301 (2021). <https://doi.org/10.1103/PhysRevLett.126.082301>
14. O. Hen, et al. In: *Medium Proton Structure Functions, SRC, and the EMC effect*. JLab PAC Proposal (2011). [https://www.jlab.org/exp\\_prog/proposals/11/PR12-11-107.pdf](https://www.jlab.org/exp_prog/proposals/11/PR12-11-107.pdf). Accessed 01 June 2024
15. B. Xiong et al., A small proton charge radius from an electron–proton scattering experiment. *Nature* **575**, 147–150 (2019). <https://doi.org/10.1038/s41586-019-1721-2>
16. D. Bhetuwal et al., Constraints on the onset of color transparency from quasielastic C12(e, e'p) up to Q<sup>2</sup>=14.2(GeV/c)<sup>2</sup>. *Phys. Rev. C* **108**(2), 025203 (2023). <https://doi.org/10.1103/PhysRevC.108.025203>. arXiv:2205.13495 [nucl-ex]

17. N. Baillie et al., Measurement of the neutron F2 structure function via spectator tagging with CLAS. *Phys. Rev. Lett.* **108**, 142001 (2012). <https://doi.org/10.1103/PhysRevLett.108.142001>. [Erratum: *Phys. Rev. Lett.* **108**, 199902 (2012)] [arXiv:1110.2770](https://arxiv.org/abs/1110.2770) [nucl-ex]
18. S. Kuhn, et al. The Structure of the Free Neutron at Large x-Bjorken. JLab PAC Proposal (2006). [https://www.jlab.org/exp\\_prog/proposals/10/PR12-06-113-pac36.pdf](https://www.jlab.org/exp_prog/proposals/10/PR12-06-113-pac36.pdf)
19. W. Melnitchouk, M. Sargsian, M.I. Strikman, Probing the origin of the EMC effect via tagged structure functions of the deuteron. *Z. Phys. A* **359**, 99–109 (1997). <https://doi.org/10.1007/s002180050372>. [arXiv:nucl-th/9609048](https://arxiv.org/abs/nucl-th/9609048)
20. W. Cosyn, M. Sargsian, Final-state interactions in semi-inclusive deep inelastic scattering off the deuteron. *Phys. Rev. C* **84**, 014601 (2011). <https://doi.org/10.1103/PhysRevC.84.014601>. [arXiv:1012.0293](https://arxiv.org/abs/1012.0293) [nucl-th]
21. C. CiofidegliAtti, L.P. Kaptari, Semi-inclusive deep inelastic scattering off few-nucleon systems: tagging the EMC effect and hadronization mechanisms with detection of slow recoiling nuclei. *Phys. Rev. C* **83**, 044602 (2011). <https://doi.org/10.1103/PhysRevC.83.044602>. [arXiv:1011.5960](https://arxiv.org/abs/1011.5960) [nucl-th]
22. A.V. Klimentenko et al., Electron scattering from high-momentum neutrons in deuterium. *Phys. Rev. C* **73**, 035212 (2006). <https://doi.org/10.1103/PhysRevC.73.035212>. [arXiv:nucl-ex/0510032](https://arxiv.org/abs/nucl-ex/0510032)
23. E.S. Smith et al., The time-of-flight system for CLAS. *Nucl. Instrum. Methods A* **432**, 265–298 (1999). [https://doi.org/10.1016/S0168-9002\(99\)00484-2](https://doi.org/10.1016/S0168-9002(99)00484-2)
24. B.A. Mecking et al., The CEBAF large acceptance spectrometer (CLAS). *Nucl. Instrum. Methods A* **503**, 513–553 (2003). [https://doi.org/10.1016/S0168-9002\(03\)01001-5](https://doi.org/10.1016/S0168-9002(03)01001-5)
25. A. Denniston et al., Laser calibration system for time of flight scintillator arrays. *Nucl. Instrum. Methods A* **973**, 164177 (2020). <https://doi.org/10.1016/j.nima.2020.164177>. [arXiv:2004.10268](https://arxiv.org/abs/2004.10268) [physics.ins-det]
26. X. Bai, Jefferson Lab High Precision Proton Radius Measurement Experiment: Prad. Ph.D. thesis, University of Virginia (2020). <https://doi.org/10.18130/v3-k8q4-z887>
27. L. Jones, APV25-S1: User guide version 2.2. RAL Microelectronics Design Group, Chilton (2001) <https://cds.cern.ch/record/1069892>
28. E.P. Segarra, J.R. Pybus, F. Hauenstein, D.W. Higinbotham, G.A. Miller, E. Piasetzky, A. Schmidt, M. Strikman, L.B. Weinstein, O. Hen, Short-range correlations and the nuclear EMC effect in deuterium and helium-3. *Phys. Rev. Res.* **3**(2), 023240 (2021). <https://doi.org/10.1103/PhysRevResearch.3.023240>. [arXiv:2006.10249](https://arxiv.org/abs/2006.10249) [hep-ph]
29. J. Arrington, J.G. Rubin, W. Melnitchouk, How well do we know the neutron structure function? *Phys. Rev. Lett.* **108**, 252001 (2012). <https://doi.org/10.1103/PhysRevLett.108.252001>. [arXiv:1110.3362](https://arxiv.org/abs/1110.3362) [hep-ph]
30. E.P. Segarra, A. Schmidt, T. Kutz, D.W. Higinbotham, E. Piasetzky, M. Strikman, L.B. Weinstein, O. Hen, Neutron valence structure from nuclear deep inelastic scattering. *Phys. Rev. Lett.* **124**(9), 092002 (2020). <https://doi.org/10.1103/PhysRevLett.124.092002>. [arXiv:1908.02223](https://arxiv.org/abs/1908.02223) [nucl-th]

Springer Nature or its licensor (e.g. a society or other partner) holds exclusive rights to this article under a publishing agreement with the author(s) or other rightsholder(s); author self-archiving of the accepted manuscript version of this article is solely governed by the terms of such publishing agreement and applicable law.